cAMP-inducible coactivator CRTC3 attenuates brown adipose tissue thermogenesis

Young-Sil Yoon[a], Wen-Wei Tsai[a,1], Sam Van de Velde[a], Zhijiang Chen[a], Kuo-Fen Lee[a], Donald A. Morgan[b], Kamal Rahmouni[b], Shigenobu Matsumura[c], Ezra Wiater[a], Youngsup Song[d], and Marc Montminy[a,2]

[a]Peptide Biology Laboratories, Salk Institute, La Jolla, CA 92037; [b]Department of Pharmacology, University of Iowa Carver College of Medicine, Iowa City, IA 52242; [c]Division of Food Science and Biotechnology, Graduate School of Agriculture, Kyoto University, 606-8502 Kyoto, Japan; and [d]Department of Medicine, Ulsan University School of Medicine, Asan Medical Center, Song Pa-gu, 138-736 Seoul, Republic of Korea

Contributed by Marc Montminy, April 23, 2018 (sent for review March 28, 2018; reviewed by Shingo Kajimura and Pere Puigserver)

In response to cold exposure, placental mammals maintain body temperature by increasing sympathetic nerve activity in brown adipose tissue (BAT). Triggering of β-adrenergic receptors on brown adipocytes stimulates thermogenesis via induction of the cAMP/PKA pathway. Although cAMP response element-binding protein (CREB) and its coactivators—the cAMP-regulated transcriptional coactivators (CRTCs)—mediate transcriptional effects of cAMP in most tissues, other transcription factors such as ATF2 appear critical for induction of thermogenic genes by cAMP in BAT. Brown adipocytes arise from Myf5-positive mesenchymal cells under the control of PRDM16, a coactivator that concurrently represses differentiation along the skeletal muscle lineage. Here, we show that the CREB coactivator CRTC3 is part of an inhibitory feedback pathway that antagonizes PRDM16-dependent differentiation. Mice with a knockout of CRTC3 in BAT (BKO) have increased cold tolerance and reduced adiposity, whereas mice overexpressing constitutively active CRTC3 in adipose tissue are more cold sensitive and have greater fat mass. CRTC3 reduced sympathetic nerve activity in BAT by up-regulating the expression of miR-206, a microRNA that promotes differentiation along the myogenic lineage and that we show here decreases the expression of VEGFA and neurotrophins critical for BAT innervation and vascularization. Sympathetic nerve activity to BAT was enhanced in BKO mice, leading to increases in catecholamine signaling that stimulated energy expenditure. As reexpression of miR-206 in BAT from BKO mice reversed the salutary effects of CRTC3 depletion on cold tolerance, our studies suggest that small-molecule inhibitors against this coactivator may provide therapeutic benefit to overweight individuals.

CREB | CRTC3 | BAT | thermogenesis

Obesity is a major risk factor for the development of insulin resistance and type II diabetes. Although diet and exercise can effectively reduce disease progression, such behavioral changes have proven difficult to implement. Because it promotes energy expenditure through nonshivering thermogenesis, brown adipose tissue (BAT) provides an attractive target for obesity treatment (1).

BAT is embryologically derived from pluripotent Myf5-positive mesenchymal cells that give rise to both skeletal myocytes and brown adipocytes (2). The coactivator PRDM16 appears critical for establishment of the brown adipocyte lineage and for repression of skeletal myocyte fate. PRDM16 stimulates the thermogenic program via an association with C/EBPβ (3). In addition, it represses skeletal muscle gene expression in part by interacting with CtBP and other repressors (4). Transgenic (Tg) expression of PRDM16 in s.c. adipose tissue enhances the thermogenic response to cold or high-fat diet (HFD) feeding by increasing sympathetic innervation, although the mechanism is unclear (5).

Functional connections between sympathetic ganglia and BAT are established during development and maintained in adulthood through the release of nerve growth factor (NGF) and other neurotrophins by brown preadipocytes (6). Indeed, Tg NGF overexpression increases BAT activity (7), while administration of neutralizing NGF antiserum reduces it (8).

β-Adrenergic stimuli have been shown to trigger the expression of cellular genes in most tissues via the PKA-mediated phosphorylation of cAMP response element-binding protein (CREB) at Ser133, a modification that promotes its interaction with the lysine acetyl-transferase (KAT) paralogs CBP and P300 (9). In parallel, cAMP also modulates CREB activity via the family of cAMP-regulated transcriptional coactivators (CRTCs) (10, 11). In the basal state, CRTCs are phosphorylated by salt-inducible kinases (SIKs) and sequestered in the cytoplasm through phosphorylation-dependent interactions with 14-3-3 proteins (12, 13). Exposure to cAMP triggers the PKA-mediated inhibition of the SIKs (14) and subsequent dephosphorylation of CRTCs. Dephosphorylated CRTCs migrate to the nucleus, where they bind to CREB over relevant promoters and stimulate recruitment of the transcriptional machinery.

CREB and CRTC3 are thought to mediate the transcriptional effects of cold exposure and HFD feeding in BAT (15, 16). Indeed, a number of promoters for thermogenic genes such as UCP1, DIO2, and PPARGC1A contain functional CREB binding sites. Moreover, CRTC3 has been reported to stimulate UCP1 gene

Significance

Physiologic systems often maintain homeostasis through negative-feedback loops. Unlike most regulatory targets for the sympathetic nervous system, interscapular brown adipose tissue (BAT) lacks parasympathetic inputs that might otherwise counterbalance the stimulatory effects of catecholamines. We found that the cAMP response element-binding protein (CREB) coactivator cAMP-regulated transcriptional coactivator 3 (CRTC3) reduces BAT function by down-regulating sympathetic nerve activity and vascularization. Mice with a knockout of CRTC3 in BAT have reduced adiposity and are more cold tolerant. CRTC3 inhibits BAT activity by disrupting the expression of neurotrophins and proangiogenic factors that otherwise promote sympathetic innervation and vascularization of BAT. These studies highlight an important feedback mechanism that maintains energy homeostasis via its effects in brown fat.

Author contributions: Y.-S.Y., K.-F.L., K.R., and M.M. designed research; Y.-S.Y., W.-W.T., S.V.d.V., Z.C., D.A.M., S.M., E.W., and Y.S. performed research; Y.-S.Y., W.-W.T., S.V.d.V., Z.C., K.-F.L., D.A.M., K.R., S.M., E.W., Y.S., and M.M. analyzed data; and Y.-S.Y. and M.M. wrote the paper.

Reviewers: S.K., University of California, San Francisco; and P.P., Dana–Farber Cancer Institute.

The authors declare no conflict of interest.

Data deposition: The data reported in this paper have been deposited in the Gene Expression Omnibus (GEO) database, https://www.ncbi.nlm.nih.gov/geo (accession no. GSE109443).

[1]Present address: Ionis Pharmaceuticals, Carlsbad, CA 92010.

[2]To whom correspondence should be addressed. Email: montminy@salk.edu.

This article contains supporting information online at www.pnas.org/lookup/suppl/doi:10.1073/pnas.1805257115/-/DCSupplemental.

Published online May 21, 2018.

expression via an association with C/EBPβ (17). However, mice with a whole-body knockout of CRTC3 actually have elevated core body temperatures and reduced adipose stores, arguing for an inhibitory role of CRTC3 in BAT (18).

To address this question, we characterized mice with a knockout of CRTC3 in Myf5-positive mesenchymal cells. We found that this coactivator modulates the thermogenic response in part through its effects on sympathetic innervation and brown adipocyte differentiation. The results provide insight into feedback regulation of BAT via a cAMP-inducible transcriptional coactivator.

Results

Increased Thermogenesis in CRTC3-Deficient Mice. To evaluate the role of CRTC3 in BAT, we crossed mice carrying a floxed allele for CRTC3 (19) with Myf5-Cre Tg mice expressing Cre recombinase in mesenchymal cells, which give rise to brown adipocytes and skeletal myocytes (2) (*SI Appendix*, Fig. S1*A*). CRTC3 mRNA and protein amounts are selectively decreased in BAT and skeletal muscle of CRTC3 BAT knockout (BKO) mice (*SI Appendix*, Fig. S1*B*). Knockout of CRTC3 has no effect on mRNA and protein amounts for CRTC1 or CRTC2 in either BAT or skeletal muscle.

Although they appear comparable to control (CRTC3 fl/fl) littermates at birth, BKO mice gain less weight and have reduced fat mass either on a normal chow (NCD) or HFD, despite a trend toward higher food intake (Fig. 1 *A*–*C*). Consistent with their reduced adiposity, BKO mice have lower circulating concentrations of leptin (Fig. 1*B*).

We performed metabolic cage studies to characterize the mechanism underlying the depletion of fat stores in BKO mice. Oxygen consumption and energy expenditure are elevated in BKO relative to control mice, particularly at night when physical activity and food intake are also increased (Fig. 1*C*). Pointing to a potential increase in sympathetic outflow, circulating concentrations of norepinephrine tend to be higher in BKO mice (Fig. 1*B*).

Following its release from sympathetic nerve terminals, norepinephrine enhances BAT activity primarily by stimulating the β3-adrenergic receptor and triggering the cAMP pathway (15). PKA activity was low in WT BAT under thermoneutral conditions by immunoblot assay using a phospho-PKA substrate antiserum (*SI Appendix*, Fig. S2*A*). Cold exposure stimulated PKA activity, leading to increases in CREB phosphorylation as well as CRTC3 dephosphorylation in WT (CRTC3 fl/fl) BAT (*SI Appendix*, Fig. S2 *B* and *C*). In keeping with the elevations in circulating norepinephrine, both basal and cold-induced PKA activity were higher in BKO BAT relative to control. PKA activity was also increased in white adipose tissue, signaling an increase in lipolysis (*SI Appendix*, Fig. S2*D*). Correspondingly, BKO mice were more tolerant to cold exposure than control littermates (Fig. 1*D*). In keeping with this apparent increase in BAT function, glucose disposal was also enhanced in BKO mice fed a high-carbohydrate diet (HCD) relative to control (Fig. 1*E*).

Because Myf5-positive mesenchymal cells can also differentiate into skeletal myocytes, we considered that the metabolic changes in BKO mice could reflect a loss of CRTC3 expression in skeletal muscle. To test this possibility, we crossed CRTC3 fl/fl mice with skeletal muscle-specific creatine kinase (Mck)-Cre Tg mice (20). Depletion of CRTC3 had no effect on body weight, cold tolerance, or treadmill running in muscle-specific knockout (MKO) mice, however (*SI Appendix*, Fig. S3 *A*–*C*). Moreover, energy expenditure and O_2 consumption were comparable between MKO and control mice, while energy expenditure was actually lower in MKO animals (*SI Appendix*, Fig. S3*D*); thermogenic gene expression in muscle was also unaffected (*SI Appendix*, Fig. S3*E*). Taken together, these results indicate that the enhanced cold tolerance in BKO mice reflects an increase in BAT function.

CRTC3 Modulates Sympathetic Innervation and Vascularization of BAT. Having seen the salutary effects of CRTC3 depletion on cold acclimation, we wondered whether overexpression of CRTC3 would have the opposite effect. Tg mice expressing modest amounts of phosphorylation-defective, constitutively active (S162A) CRTC3 protein (21), under control of an adipose-specific (aP2) promoter, had increased fat mass on a NCD (*SI Appendix*, Fig. S4*A*). BAT tissue from NCD-fed CRTC3 Tg animals appeared pale, with lipid-laden brown adipocytes (*SI Appendix*, Fig. S4*B*). Free fatty acid and triglyceride amounts in BAT were elevated in CRTC3 Tg mice, suggesting a disruption in fatty acid oxidation (*SI Appendix*, Fig. S4*B*). Correspondingly, CRTC3 Tg mice have impaired cold tolerance relative to control littermates (*SI Appendix*, Fig. S4*C*).

Based on the increases in circulating NE concentrations and PKA activity in BAT from BKO mice, we wondered whether CRTC3 modulates either sympathetic innervation or catecholamine signaling in this tissue. Staining for the catecholamine biosynthetic enzyme tyrosine hydroxylase (TH) was elevated in BKO BAT with more extensive varicosities that are often indicative of increased parenchymal innervation (Fig. 2*A*). β3-Adrenergic receptor (ADRB3) staining was also up-regulated in BKO BAT relative to control. By contrast, TH and ADRB3 protein amounts were decreased in BAT from CRTC3 Tg mice (*SI Appendix*, Fig. S5).

Having seen that CRTC3 modulates sympathetic innervation to BAT, we tested whether sympathetic nerve activity (SNA) is correspondingly elevated in BKO mice. Baseline SNA at 37 °C was modestly reduced in BKO relative to WT animals [0.66 (±0.05) vs. 0.4 (±0.02) V·s/min]. Although gradual cooling increased SNA in both groups, it did so more robustly in BKO mice relative to control (Fig. 2B and *SI Appendix*, Fig. S6). SNA was not globally elevated, however, as heart rate and blood pressure were comparable between BKO and controls (*SI Appendix*, Fig. S6*B*).

In addition to effects of sympathetic innervation, vascularization of BAT is critical for its thermogenic function (22). Cold exposure triggers VEGFA-dependent increases in blood flow that facilitate the delivery of metabolic substrates to BAT for heat generation (22, 23). Indeed, cold exposure increased capillary density in WT BAT, as revealed by immunohistochemistry using the angiogenic marker CD31 (24). BAT vascularity was elevated in BKO mice relative to controls following cold exposure (Fig. 2C); it was reduced in BAT from CRTC3 Tg mice compared with WT littermates (*SI Appendix*, Fig. S5*B*), demonstrating that CRTC3 modulates BAT function through its effects on both sympathetic tone and capillary density.

Sympathetic innervation of BAT is guided by NGF as well as other neurotrophins that are produced by brown preadipocytes (25). Addition of crude BAT extract from BKO mice stimulated neurite extension from cultured superior cervical ganglia (SCGs) to a greater extent than extract from control BAT (Fig. 2*D*). Addition of neutralizing antisera against NGF, BDNF, or the angiogenic factor VEGFA, which can also function as a neurotrophin (26, 27), reduced neurite outgrowth (Fig. 2*E*, *Bottom*). In keeping with these results, protein amounts for NGF, BDNF, as well as VEGFA were increased in BKO BAT relative to control (Fig. 2*E*, *Top*).

CRTC3 Modulates Brown Preadipocyte Differentiation. By contrast with the inhibitory effects of CRTC3, PRDM16 has been shown to promote expression of the thermogenic program in BAT (5), suggesting that these coactivators function antagonistically. Supporting this idea, exposure of BKO brown adipose stromal vascular fraction cells (bSVFs) to differentiation mixture stimulated Oil Red O staining more readily than control bSVFs (Fig. 3*A*). By contrast, exposure to mixture had minimal effects on Oil Red O staining of bSVFs from CRTC3 Tg mice. In keeping with these effects, mRNA and protein amounts for thermogenic genes such as UCP1 were up-regulated in differentiated BKO

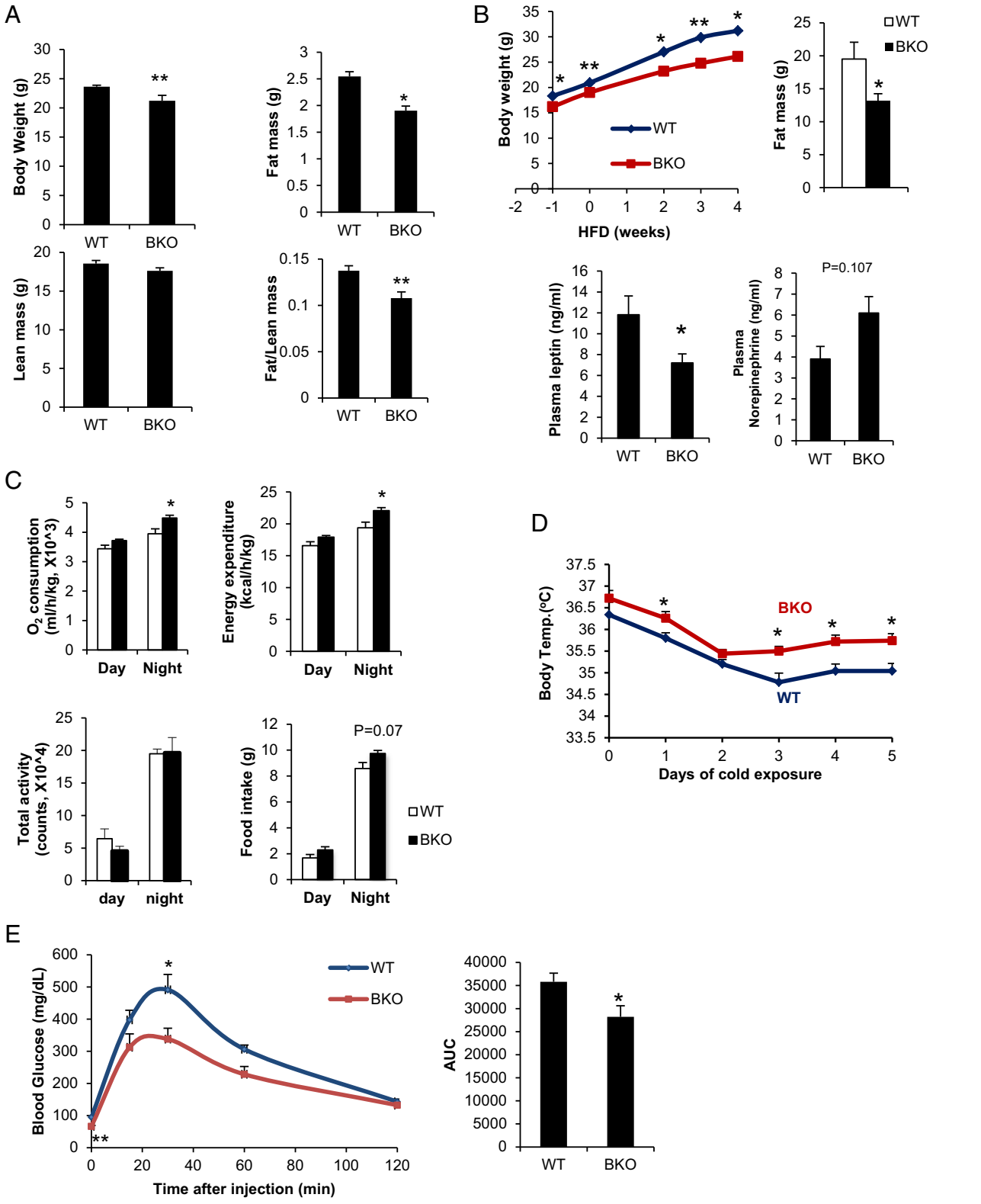

Fig. 1. Depletion of CRTC3 in BAT increases thermogenesis. (*A*) Body weight and fat mass of ad libitum-fed 10-wk-old WT control (CRTC3 fl/fl) and CRTC3 BAT knockout (BKO) mice on a normal chow diet (NCD). $n = 3$ and 5 per group. (*B*, *Top*) Effect of high-fat diet (HFD) on body weight (after 4 wk) and fat mass (after 12 wk) in BKO mice and control littermates. (*B*, *Bottom*) Circulating concentrations of leptin and norepinephrine in HFD-fed (after 4 wk) mice. $n = 4$ and 7 per group. (*C*) Indirect calorimetric analysis of BKO and control littermates, monitored for 48 h following cage adaptation. $n = 4$ per group. (*D*) Core body temperatures in NCD-fed control and CRTC3 BKO mice following cold exposure (4–5 °C) for times indicated. $n = 5$ per group. (*E*) Glucose tolerance test (GTT) (1.5 g/kg glucose) of high-carbohydrate diet (HCD) (16 wk)-fed mice. $n = 6$ and 8 per group. (*Right*) Area under curve for GTT. Data for *A*–*E* represent means ± SEM (*$P < 0.05$; **$P < 0.01$).

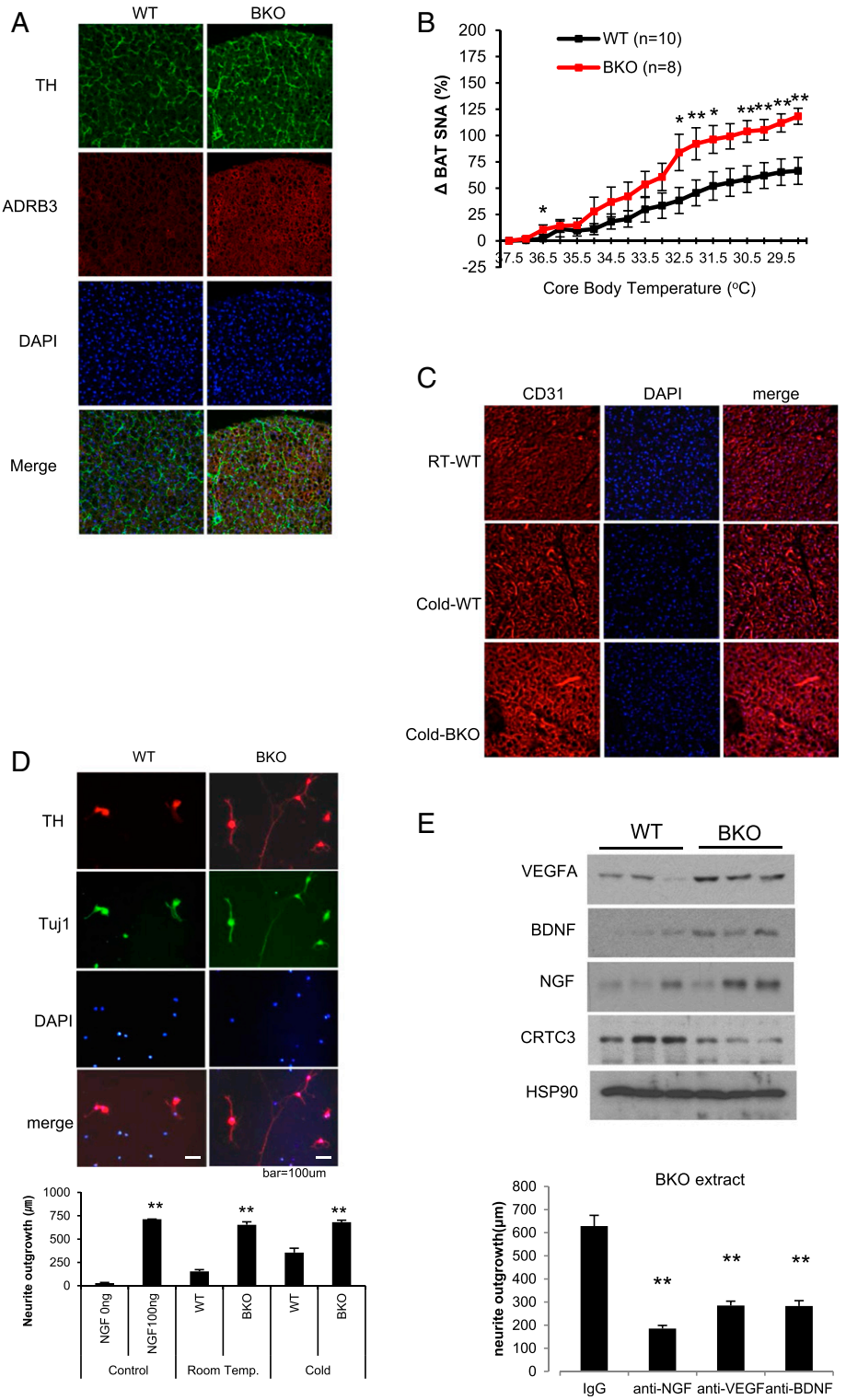

Fig. 2. Increased sympathetic innervation and vascularization of BAT in BKO mice. (*A*) Immunofluorescence analysis of tyrosine hydroxylase (TH) and β3 adrenergic receptor (ADRB3) expression in BAT from WT (CRTC3 fl/fl) and BKO littermates at ambient temperature. Representative images from three independent experiments shown. (*B*) Sympathetic nerve activity (SNA) to BAT, measured by direct recording of nerve fibers in response to decreasing core body temperature of NCD-fed WT and CRTC3 BKO mice. $n = 10$ and 8 per group. Data represent means ± SEM. (*C*) Immunofluorescence analysis showing effect of cold exposure (15 h) on BAT vascularization in WT and BKO mice using the angiogenic marker CD31. Images are representative of three different experiments. (*D*, *Top*) Immunofluorescence analysis of cultured neurons from SCGs showing relative effects of adding WT or BKO BAT extract on neurite extension. Cells were exposed to crude extracts for 18 h and then stained with anti-TH and Tuj1 antibody to visualize sympathetic neurons. Representative images are shown. (*D*, *Bottom*) Bar graph showing relative neurite outgrowth in cells exposed to BAT extract from BKO and WT mice. Exposure to cold (3 h) indicated. $n = 30–120$. (*E*, *Top*) Immunoblot showing relative protein amounts for neurotrophic factors (NGF, BDNF, VEGFA) in brown-fat extracts from WT and BKO mice. $n = 3$ per group. (*E*, *Bottom*) Effect of anti-VEGFA, anti-BDNF, and anti-NGF neutralizing antibodies on neurite extension in response to addition of BKO BAT extract. $n = 95–122$ ($^*P < 0.05$; $^{**}P < 0.01$).

bSVFs relative to control bSVFs, while mRNA amounts for skeletal muscle genes were preferentially decreased in BKO bSVFs (Fig. 3 *B* and *C*). Indeed, skeletal muscle-related genes were the top-scoring group of genes that are down-regulated in BKO bSVFs by RNA-sequencing (RNA-seq) analysis (*SI Appendix*, Fig. S7). Skeletal muscle gene expression was also reduced in BKO BAT relative to control, whereas mRNA amounts for thermogenic factors such as PPARGC1A and PRDM16 were elevated (*SI Appendix*, Fig. S8).

PRDM16 has been shown to promote the differentiation of bSVFs and other cells, perhaps most notably skeletal myoblasts, into brown adipocytes (2). Stable overexpression of PRDM16 in C2C12 myoblasts stimulated their differentiation into brown adipocytes following their exposure to mixture (Fig. 3*D*). Modest CRTC3 overexpression in PRDM16-expressing C2C12 (PRDM16-C2C12) cells blocked their differentiation to brown adipocytes (Fig. 3*D*). Indeed, mRNA and protein amounts for thermogenic genes (UCP1, C/EBPβ, PPARγ) were down-regulated following overexpression of CRTC3 in C2C12-PRDM16 cells (Fig. 3*E*). Conversely, CRTC3 overexpression stimulated increases in mRNA amounts for skeletal muscle genes (MEF2, MyoD1, MyoG), demonstrating that CRTC3 antagonizes both stimulatory and inhibitory aspects of PRDM16 function in this setting.

Mir-206 Mediates Effects of CRTC3 in BAT. In the process of addressing the mechanism by which CRTC3 overexpression stimulates the skeletal muscle program, we noted that RNA amounts for miR-206, a microRNA that increases skeletal muscle gene expression (28, 29), are up-regulated in brown preadipocytes from CRTC3 Tg mice; they are decreased in CRTC3-deficient BKO preadipocytes (Fig. 4*A*). The miR-206 promoter contains a consensus CREB binding site; and exposure of bSVFs to Fsk triggered CRTC3 recruitment to this regulatory element by chromatin immunoprecipitation (ChIP) assay (Fig. 4*B*). In transient luciferase assays of HIB1B brown preadipocytes, exposure to Fsk stimulated miR-206 promoter activity, and CRTC3 overexpression further augmented this response (Fig. 4*C*). Disrupting CREB binding, either by coexpressing the dominant-negative CREB inhibitor A-CREB (30) or by mutating the CREB binding site on the miR-206 promoter, reduced reporter expression. Correspondingly, protein amounts for skeletal muscle regulators (MYOD, SRF, MEF2) are reduced in BKO BAT; these effects are reversed by miR-206 overexpression (*SI Appendix*, Fig. S9*A*).

In addition to its role in stimulating skeletal muscle gene expression, miR-206 has also been reported to inhibit VEGFA production in zebrafish (31). The presence of a conserved miR-206 targeting site in the 3′-UTR of mammalian VEGFA genes (*SI Appendix*, Fig. S9*B*) prompted us to test whether miR-206 modulates VEGFA expression in brown preadipocytes. Overexpression of miR-206 in HIB1B cells decreased the activity of a VEGFA-luciferase fusion gene containing the miR-206 binding site but not a mutant fusion gene lacking this site (*SI Appendix*, Fig. S9*B*). Consistent with these results, overexpression of adeno-associated virus (AAV)-encoded miR-206 reduced VEGFA secretion from both WT and BKO bSVFs (Fig. 4*D*), suggesting that CRTC3 reduces BAT vascularization by stimulating miR-206 expression and thereby downregulating VEGFA production.

In addition to VEGFA, the BDNF and NGF genes contain full and partial miR-206 targeting sites, respectively (32). Correspondingly, NGF and BDNF release were both increased in BKO bSVFs relative to control, while miR-206 overexpression in bSVFs decreased NGF and BDNF secretion (*SI Appendix*, Fig. S9*C*). Indeed, administration of AAV-miR-206 virus into interscapular BAT (iBAT) from BKO mice reduced protein amounts for all three neurotrophins (Fig. 4*E*, *Left*). These results indicate that miR-206 is important in mediating inhibitory effects of CRTC3 on neurotrophin expression.

TH protein amounts were also down-regulated following miR-206 overexpression in BAT, pointing to a decrease in sympathetic nerve density (Fig. 4*E*, *Left*). As a result, AAV-miR-206 expression in iBAT of BKO mice lowered core body temperature to WT levels following cold exposure (Fig. 4*E*, *Right*), demonstrating the importance of miR-206 in mediating inhibitory effects of CRTC3 on BAT activity.

Discussion

Physiologic systems often maintain homeostasis through negative-feedback loops that attenuate the response to inductive signals. Unlike most regulatory targets for the sympathetic nervous system, however, iBAT lacks parasympathetic inputs that might otherwise counterbalance the stimulatory effects of catecholamines on adaptive thermogenesis. Here, we show how a transcriptional coactivator that is itself regulated by cAMP attenuates adaptive thermogenesis in BAT (*SI Appendix*, Fig. S10).

We found that CRTC3 reduces BAT activity by downregulating SNA and vascularization. The effects of CRTC3 appear to be paracrine in nature, involving the release of VEGFA as well as NGF and BDNF from brown adipocytes. Future studies should address the importance of these factors in modulating sympathetic innervation in adult BAT.

Superimposed on its paracrine effects, CRTC3 also appears to disrupt preadipocyte differentiation via a cell-autonomous mechanism. Although our results indicate that miR-206 mediates these inhibitory effects, CRTC3 may also interfere with expression of the thermogenic program by associating with PRDM16 and blocking its interaction with C/EBPβ.

In addition to CRTC3, BAT activity is also negatively regulated by the K^+ channel KCNK3 (33), a target gene for PRDM16 that reduces catecholamine signaling by increasing potassium efflux from brown adipocytes. Although the relative contributions of CRTC3 and KCNK3 remain unclear, we imagine that these and perhaps other factors function importantly in promoting energy balance by attenuating the thermogenic response.

Materials and Methods

Knockout Mice. CRTC3 floxed allele was generated by injection of targeted embryonic stem cells from the international Knockout Mouse Project into blastocysts of C57BL/6 mice to obtain chimeras. The CRTC3 floxed allele contains loxP sites flanking *crtc3* exon 4 and contains a *neo* cassette flanked by FRT sites as a selective marker. After germ-line transmission, the mice were crossed to mice harboring flp recombinase to excise the *neo* cassette. The floxed CRTC3 ($crtc3^{fl/+}$) mice were backcrossed to C57BL/6 mice for over five generations.

Genotyping. Genotyping of the CRTC3 floxed allele was performed using the following primers manually: forward, GCA GGC CAA GGA GAA GCT CCA TCT, and reverse, CAG GTG CTG TGA AGA ATA ACT GGC TG. Primers for CRE recombinase Tg lines were used as suggested by The Jackson Laboratory.

Animal Studies. All animal procedures were performed with an approved protocol from the Salk Institute Animal Care and Use Committee. Mice were housed in a temperature-controlled environment under 12-h light/12-h dark cycle with freely accessible water and standard rodent chow diet (Lab Diet 5001). For HFD or HCD, 5- to 7-wk-old mice were transferred to 60% fat diet (D12492; Research Diets) or 73% carbohydrate diet (AIN-93M; Research Diet), respectively. Core body temperature of mice was measured after cold exposure in a cold chamber (Percival Scientific) by thermometer (Cole-Parmer Instrument Company). Body fat and lean mass were measured using Echo MRI-100 body composition analyzer.

Primary bSVF. iBAT from 10 mice was collected, minced, and digested for 30–60 min in collagenase buffer [100 mM Hepes, pH 7.4, 1.5 mg/mL collagenase I (Sigma; C6885), 125 mM NaCl, 5 mM KCl, 1.3 mM, $CaCl_2$, 5 mM D-glucose, and 2% BSA] with gentle shaking at 37 °C. After digestion, the tissue was centrifuged at 500 × *g* for 10 min to separate floating mature adipocytes from the SVF cells. SVF cells were filtered through a 40-μm cell strainer (BD Falcon). After centrifugation, SVF cells were resuspended in RBC lysis buffer (0.017 M Tris, pH 7.4, 0.16 M NH_4Cl, and 0.01 M EDTA) and incubated for 10 min at room temperature. Suspension cells were centrifuged, washed with culture media (DMEM containing 10% FBS and 1% penicillin/streptomycin), and then plated. For differentiation studies, cells were incubated in culture media for 48 h after reaching confluence. Media was replaced with culture media containing 5 ng/mL insulin, 1 μM dexamethasone, 115 μg/mL IBMX, 0.125 mM indomethacin, 100 nM rosiglitazone, and 10 nM

BIOCHEMISTRY

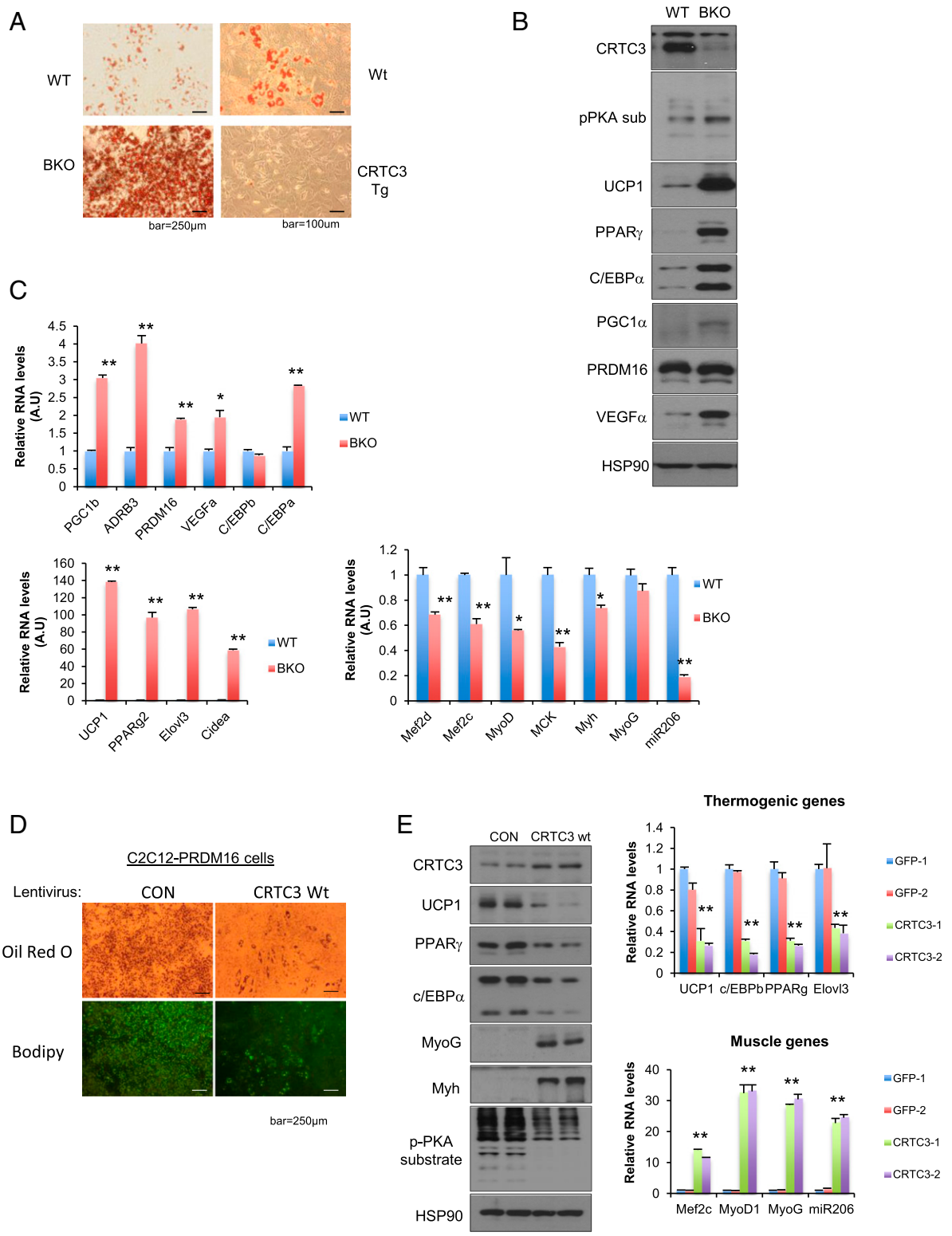

Fig. 3. Antagonistic effects of CRTC3 on PRDM16-mediated brown preadipocyte differentiation. (*A*, *Left*) Oil Red O staining of cells from the brown stromal vascular fraction (bSVFs) of BKO versus WT (CRTC3 fl/fl) littermates following exposure to differentiation mixture for 7 d. (*A*, *Right*) Oil Red O staining of bSVFs from CRTC3 Tg and WT littermates following exposure to differentiation mixture. (*B* and *C*) Relative protein (*B*) and mRNA (*C*) amounts for thermogenic and myogenic genes in differentiated bSVFs from BKO and WT littermates. (*D*) Oil Red O and BODIPY staining of C2C12 cells stably expressing PRDM16 after exposure to differentiation mixture for 7 d. Effect of lentiviral CRTC3 overexpression on differentiation of C2C12-PRDM16 cells relative to GFP control shown. (*E*) Effect of modest CRTC3 overexpression on protein (*Left*) and mRNA (*Right*) amounts for thermogenic and myogenic genes in differentiated C2C12-PRDM16 cells. Data in *C* and *E* represent means ± SD (*$P < 0.05$; **$P < 0.01$).

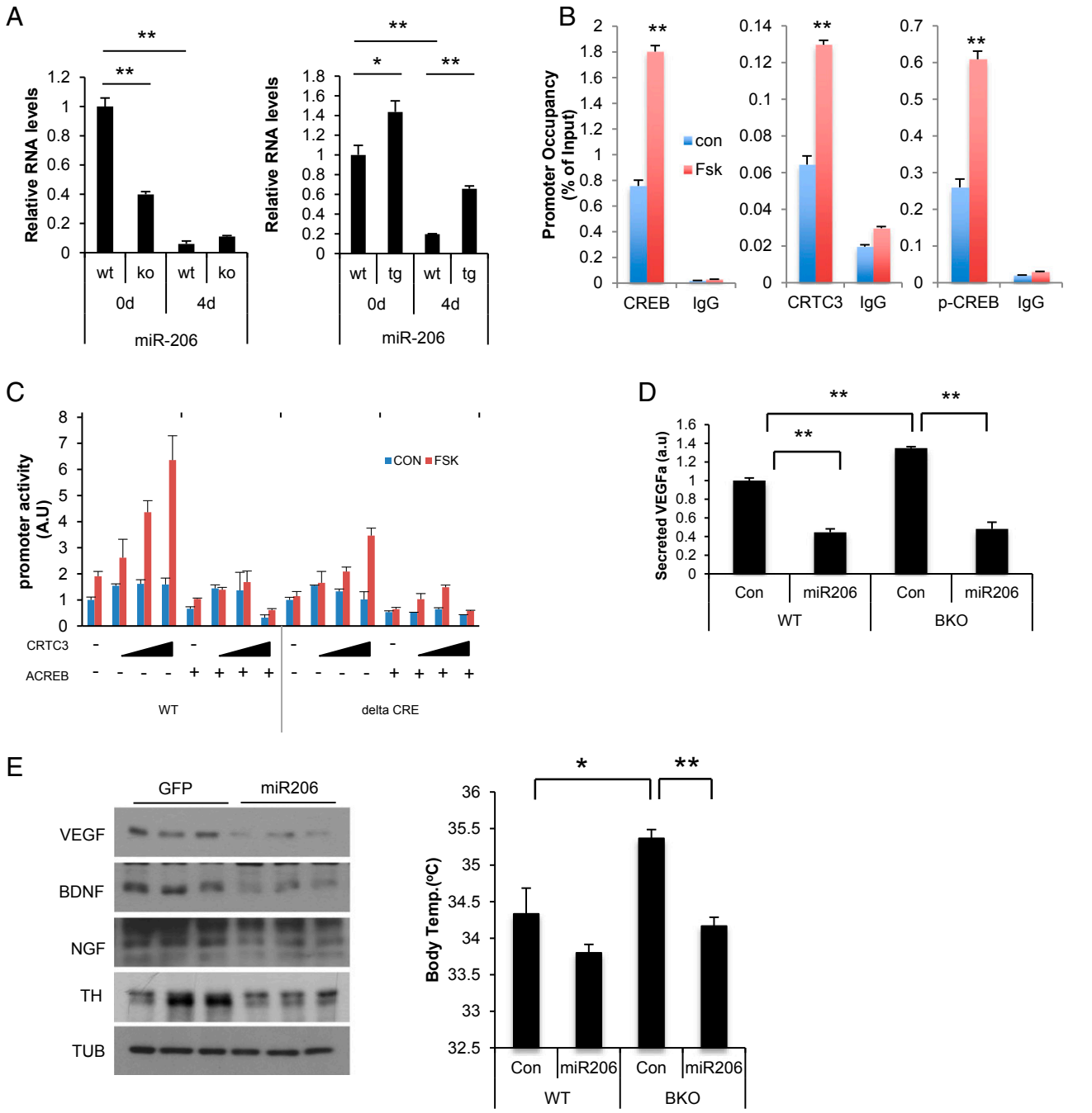

Fig. 4. miR-206 mediates inhibitory effects of CRTC3 on adaptive thermogenesis. (*A*) Effect of differentiation mixture (4 d) on RNA amounts for miR-206 in bSVFs prepared from BKO or CRTC3 Tg mice compared with respective control littermates. (*B*) Occupancy of CRTC3, CREB, and phospho (Ser133)-CREB over a CREB binding site on the miR-206 promoter in WT bSVFs under basal conditions and following exposure to FSK (light blue) for 1 h by manual ChiP assay. (*C*) Transient assay of HIB1B preadipocytes showing effects of CRTC3 or dominant-negative ACREB expression on WT and cAMP response element (ΔCRE) mutant miR-206 promoter constructs in cells exposed to FSK as indicated. $n = 3$ per group. (*D*) Effect of miR-206 on VEGFA secretion from cultured BKO or WT bSVFs infected with adenoassociated virus (AAV)-encoded miR-206 or AAV-GFP control virus. $n = 3$ per group. (*E*, *Left*) Immunoblot showing protein amounts for VEGFA, BDNF, and NGF in BAT from BKO and littermate control mice injected with AAV-miR-206 or AAV-GFP control virus into iBAT. (*E*, *Right*) Effect of AAV-miR-206 or control AAV-GFP injection into BAT on core body temperature following 4-h cold exposure in BKO and control mice. $n = 4$ per each group. Data in *A* and *C* represent means ± SD. Data in *D* and *E* represent means ± SEM (*$P < 0.05$; **$P < 0.01$).

T3 for 2 d and changed with culture media containing 5 ng/mL insulin, 100 nM rosiglitazone, and 10 nM T3 every 2 d. Cells were maintained in this differentiation medium for 8–10 d.

qRT-PCR Analysis. Total RNA was isolated using TRIzol reagent (Invitrogen), and 1–2 μg of RNA was used to make cDNA with Transcriptor first-strand cDNA synthesis kit according to the manufacturer's instruction (Roche). Relative mRNA expression was determined with SYBR green master mix (Roche) by LightCycler 480 qPCR machine (Roche). For mature miRNA detection, total RNA was polyadenylated with *Escherichia coli* poly(A) polymerase according to the manufacturer's instruction (New England Biolab) and then used for reverse transcription and qRT-PCR with specific primers (34). Relative mRNA expression was calculated by $2^{-\Delta\Delta CT}$ methods. L32 and U6 mRNA were used as housekeeping genes for mRNA and miRNA, respectively.

RNA-seq. RNA-seq libraries were constructed using NEBNext-Ultra kits (New England Biolab) according to the manufacturer's instructions. Quantitation of libraries was done by Qubit (Invitrogen) and run on a MiSeq instrument with paired-end 75-bp reads using v3 chemistry (Illumina). Data were analyzed by tophat2 and cuffdiff against the mouse mm10 genome build. Gene ontology enrichment analysis was performed on differentially expressed genes. The National Center for Biotechnology Information Gene Expression Omnibus accession number for RNA-seq studies is GSE109443.

SNA and Neurite Outgrowth. SNA was analyzed by direct recoding of spike frequency from nerve fibers innervating iBAT as described previously (35). Neurite outgrowth assays were performed as described (36). SCGs were isolated by excision under a dissecting microscope from postnatal day 0 (P0) to P2 mice. Isolated SCG neurons were plated on coverslips in 24-well cell culture plate in B27-containing Neurobasal medium (Invitrogen). Eighteen to ∼36 h postplating, cells were stained with anti-TH and Tuj1 antibodies for staining of sympathetic nerves. Neurite lengths were measured for at least 100 cells per group with ImageJ software (National Institutes of Health). For immune-neutralization studies, anti-VEGF antibody and control IgG (Biolegend), anti-BDNF antibody (Millipore), anti-NGF antibody, and control IgG (Abcam) were used.

Indirect Calorimetry. Mice fed with normal chow diet or 60% HFD for 2 mo were individually housed for at least 2 d before calorimetry experiments. Oxygen consumption, energy expenditure, food intake, and locomotor activity were simultaneously measured with a LabMaster system (TSE Systems). Data were recorded for 2–3 d and analyzed.

Viruses. CMV-miR-206 (OriGene) was subcloned into adenoviral vector and amplified and then purified as described (37). CMV-GFP, CMV-miR-206, and CMV-CRTC3 were subcloned into serotype 8 AAV vector (University of California, San Diego, Viral Core). Amplification and purification of AAVs were performed by Salk GT3 (Gene Transfer Targeting and Therapeutics) Core. For generation of stable PRDM16-C2C12 cell lines, pMSCV-Prdm16 or control vector was transfected into HEK293 cells, along with packaging vector pEco. After 48 h, supernatants containing retroviral particles were collected, filtered, and mixed with 8 μg/mL polybrene. Mixtures were added to C2C12 myoblast cells and incubated up to 48 h. Transfected cells were selected by puromycin treatment. For lentivirus, pHRST-ctrl and pHRST-CRTC3 (for CRTC3 overexpression) and lenti-US and lenti CRTC3i (for CRTC3 knockdown) along with lentiviral packaging plasmids were transfected and amplified in HEK293 cells.

AAV Injection into BAT. Mice (8–12 wk old) were anesthetized with isoflurane and hair was trimmed around iBAT. Small incision was made to the skin to expose the BAT. Five microliters of AAV for each lobe were slowly injected into BAT using a 10-μL Hamilton syringe. The skin was closed with absorbable surgical suture (Ethicon). Experiments were performed at least 2 wk after injection.

Glucose Tolerance Test. Blood glucose levels were measured from animals that were fasted for 16 h with free access to water. For glucose tolerance testing, mice were injected i.p. with glucose (1.5 g/kg of body weight for HCD-fed mice) after 16 h of fasting; blood glucose levels were measured at time points indicated.

Immunoblotting. Antibodies for immunoblotting were purchased from Cell Signaling Technologies (CRTC3, p-PKA substrate, p-CREB, PPARγ, c/EBPα), Santa Cruz Biotechnology (c/EBPβ, MyoG, MyoD, Myh, BDNF, VEGFα, NGF, PRDM16, SRF, Hsp90), Sigma (UCP1), Lifespan Bioscience (ADRB3), Millipore (PRDM16, α-tubulin), Immunostar (TH), Biolegend (c/EBPβ), and custom-made (PGC1α, CREB, p-CREB).

Luciferase Assay. *psiCheck2* carrying luciferase gene fused to a fragment of VEGFA–3′-UTR harboring miR-206 putative recognition sites were cotransfected to HIB1B cells, along with control miRNA or miR-206 (OriGene). The deleted 3′-UTR of VEGFA was generated by directed mutagenesis of the miR-206 seed region (ACAUUCC) with PrimSTAR (Clontech). Samples were collected at 48 h posttransfection. Luciferase activity was measured and normalized to RSV-β-gal activity.

Histology and Immunohistochemistry. For H&E staining, tissues were fixed in Z-Fix (Anatech) fixative, dehydrated, and embedded in paraffin. Five- to ∼10-μm sections were stained with H&E and then imaged by light microscopy (Nikon). For immunofluorescence staining, mice were anesthetized with isoflurane and perfused via aorta with PBS and chilled 4% paraformaldehyde in phosphate buffer (pH 7.0). Brown fat was dissected, stored overnight in 25% sucrose, embedded in OCT compound, and cut at 15∼30 μm using a cryostat and collected on slides. Slides were washed in 0.1 M phosphate buffer, blocked in 3% normal goat serum with 0.2% Triton X-100 made in 0.1 M phosphate buffer for 1 h, and then incubated overnight at 4 °C in primary antibodies diluted in blocking solution. Slides were washed in 0.1 M phosphate buffer and incubated 1 h in appropriate secondary antibodies diluted in blocking buffer. The following primary antibodies were used: CD31 (1:500; Abcam), ADRB3 (1:250; Lifespan), P (Ser133)-CREB (1:500; Cell Signaling), anti-TH (1:500; Immunostar), and DAPI (Sigma-Aldrich).

Oil Red O Staining. Differentiated SVF cells from BAT were washed twice with PBS and fixed with 3.7% formaldehyde in PBS for 1 h. Fixed cells were rinsed with dH_2O and 50% isopropanol. Cells were stained with 40% isopropanol containing 0.3% Oil Red O solution for 1∼2 h. Boron-dipyrromethene (BODIPY) staining was performed according to the manufacturer's instruction (D3922; Molecular Probes).

Assays. Free fatty acid and triglyceride levels were measured in brown fat following extraction by the Folch method using a BioVision colorimetric quantification kit according to the manufacturer's recommendation. The levels of plasma leptin and norepinephrine in WT and BKO mice were measured by ELISA kit from Millipore and Cloud-Clone Corporation, respectively, according to the manufacturer's protocol. Levels of secreted NGF (Millipore), BDNF (Bosterbio), and VEGFA (Millipore) were measured by ELISA according to the manufacturer's protocol.

Statistical Analysis. Data are presented with mean ± SEM or mean ± SD as indicated. *P* values were calculated using two-tailed Student's *t* test. Data points with value of $P < 0.05$ were considered to be statistically significant. Statistical significance was indicated as $*P < 0.05$ and $**P < 0.01$.

ACKNOWLEDGMENTS. This work was supported by NIH Grants R01 DK083834 (to M.M.), AG047669 (to K.-F.L.), MH114831 (to K.-F.L.), OD023076 (to K.-F.L.), HL084207 (to K.R.), and CA014195 (to K.-F.L.); the Leona M. and Harry B. Helmsley Charitable Trust (M.M.); the Clayton Foundation for Medical Research (M.M. and K.-F.L.); The Don and Lorraine Freeberg Foundation (K.-F.L.); and the Kieckhefer Foundation (M.M.). Y.-S.Y. is supported by Grant HI11C1941 from the Ministry of Health and Welfare (Korea). This work was also supported by the American Heart Association Award 14EIA18860041 (to K.R.), the University of Iowa Fraternal Order of Eagles Diabetes Research Center (K.R.), and the University of Iowa Center for Hypertension Research (K.R.).

1. Chechi K, Nedergaard J, Richard D (2014) Brown adipose tissue as an anti-obesity tissue in humans. *Obes Rev* 15:92–106.
2. Seale P, et al. (2008) PRDM16 controls a brown fat/skeletal muscle switch. *Nature* 454: 961–967.
3. Kajimura S, et al. (2009) Initiation of myoblast to brown fat switch by a PRDM16-C/EBP-beta transcriptional complex. *Nature* 460:1154–1158.
4. Ohno H, Shinoda K, Ohyama K, Sharp LZ, Kajimura S (2013) EHMT1 controls brown adipose cell fate and thermogenesis through the PRDM16 complex. *Nature* 504:163–167.
5. Seale P, et al. (2011) Prdm16 determines the thermogenic program of subcutaneous white adipose tissue in mice. *J Clin Invest* 121:96–105.
6. Chaldakov GN, Tonchev AB, Aloe L (2009) NGF and BDNF: From nerves to adipose tissue, from neurokines to metabokines. *Riv Psichiatr* 44:79–87.
7. Hansen-Algenstaedt N, et al. (2006) Neural driven angiogenesis by overexpression of nerve growth factor. *Histochem Cell Biol* 125:637–649.
8. Gorin PD, Johnson EM, Jr (1980) Effects of long-term nerve growth factor deprivation on the nervous system of the adult rat: An experimental autoimmune approach. *Brain Res* 198:27–42.
9. Altarejos JY, Montminy M (2011) CREB and the CRTC co-activators: Sensors for hormonal and metabolic signals. *Nat Rev Mol Cell Biol* 12:141–151.
10. Conkright MD, et al. (2003) TORCs: Transducers of regulated CREB activity. *Mol Cell* 12:413–423.
11. Iourgenko V, et al. (2003) Identification of a family of cAMP response element-binding protein coactivators by genome-scale functional analysis in mammalian cells. *Proc Natl Acad Sci USA* 100:12147–12152.
12. Bittinger MA, et al. (2004) Activation of cAMP response element-mediated gene expression by regulated nuclear transport of TORC proteins. *Curr Biol* 14:2156–2161.
13. Li HX, Xiao L, Wang C, Gao JL, Zhai YG (2010) Review: Epigenetic regulation of adipocyte differentiation and adipogenesis. *J Zhejiang Univ Sci B* 11:784–791.
14. Sonntag T, Vaughan JM, Montminy M (2018) 14-3-3 proteins mediate inhibitory effects of cAMP on salt-inducible kinases (SIKs). *FEBS J* 285:467–480.
15. Cannon B, Nedergaard J (2004) Brown adipose tissue: Function and physiological significance. *Physiol Rev* 84:277–359.
16. Hatting M, et al. (2017) Adipose tissue CLK2 promotes energy expenditure during high-fat diet intermittent fasting. *Cell Metab* 25:428–437.

17. Shan T, et al. (2016) Lkb1 controls brown adipose tissue growth and thermogenesis by regulating the intracellular localization of CRTC3. *Nat Commun* 7:12205.
18. Song Y, et al.; CHARGE Consortium; GIANT Consortium (2010) CRTC3 links catecholamine signalling to energy balance. *Nature* 468:933–939.
19. Luan B, et al. (2015) CREB pathway links PGE2 signaling with macrophage polarization. *Proc Natl Acad Sci USA* 112:15642–15647.
20. Huh MS, Parker MH, Scimè A, Parks R, Rudnicki MA (2004) Rb is required for progression through myogenic differentiation but not maintenance of terminal differentiation. *J Cell Biol* 166:865–876.
21. Sonntag T, et al. (2017) Analysis of a cAMP regulated coactivator family reveals an alternative phosphorylation motif for AMPK family members. *PLoS One* 12:e0173013.
22. Sun K, et al. (2014) Brown adipose tissue derived VEGF-A modulates cold tolerance and energy expenditure. *Mol Metab* 3:474–483.
23. During MJ, et al. (2015) Adipose VEGF links the white-to-brown fat switch with environmental, genetic, and pharmacological stimuli in male mice. *Endocrinology* 156: 2059–2073.
24. Xue Y, Lim S, Bråkenhielm E, Cao Y (2010) Adipose angiogenesis: Quantitative methods to study microvessel growth, regression and remodeling in vivo. *Nat Protoc* 5:912–920.
25. Fargali S, et al. (2012) Role of neurotrophins in the development and function of neural circuits that regulate energy homeostasis. *J Mol Neurosci* 48:654–659.
26. Sondell M, Sundler F, Kanje M (2000) Vascular endothelial growth factor is a neurotrophic factor which stimulates axonal outgrowth through the flk-1 receptor. *Eur J Neurosci* 12:4243–4254.
27. Sondell M, Lundborg G, Kanje M (1999) Vascular endothelial growth factor has neurotrophic activity and stimulates axonal outgrowth, enhancing cell survival and Schwann cell proliferation in the peripheral nervous system. *J Neurosci* 19:5731–5740.
28. Rao PK, Kumar RM, Farkhondeh M, Baskerville S, Lodish HF (2006) Myogenic factors that regulate expression of muscle-specific microRNAs. *Proc Natl Acad Sci USA* 103: 8721–8726.
29. Liu N, et al. (2012) microRNA-206 promotes skeletal muscle regeneration and delays progression of Duchenne muscular dystrophy in mice. *J Clin Invest* 122: 2054–2065.
30. Ahn S, et al. (1998) A dominant-negative inhibitor of CREB reveals that it is a general mediator of stimulus-dependent transcription of *c-fos*. *Mol Cell Biol* 18:967–977.
31. Stahlhut C, Suárez Y, Lu J, Mishima Y, Giraldez AJ (2012) miR-1 and miR-206 regulate angiogenesis by modulating VegfA expression in zebrafish. *Development* 139: 4356–4364.
32. Miura P, Amirouche A, Clow C, Bélanger G, Jasmin BJ (2012) Brain-derived neurotrophic factor expression is repressed during myogenic differentiation by miR-206. *J Neurochem* 120:230–238.
33. Chen Y, et al. (2017) Crosstalk between KCNK3-mediated ion current and adrenergic signaling regulates adipose thermogenesis and obesity. *Cell* 171:836–848.e13.
34. Liu W, et al. (2012) Hypoxia promotes satellite cell self-renewal and enhances the efficiency of myoblast transplantation. *Development* 139:2857–2865.
35. Rahmouni K, Morgan DA (2007) Hypothalamic arcuate nucleus mediates the sympathetic and arterial pressure responses to leptin. *Hypertension* 49:647–652.
36. Bengoechea TG, Chen Z, O'Leary DA, Masliah E, Lee KF (2009) p75 reduces beta-amyloid-induced sympathetic innervation deficits in an Alzheimer's disease mouse model. *Proc Natl Acad Sci USA* 106:7870–7875, and erratum (2009) 106:20134.
37. Koo SH, et al. (2004) PGC-1 promotes insulin resistance in liver through PPAR-alpha-dependent induction of TRB-3. *Nat Med* 10:530–534.